Journal of Analytical and Applied Pyrolysis 191 (2025) 107151

Contents lists available at ScienceDirect

Journal of Analytical and Applied Pyrolysis

journal homepage: www.elsevier.com/locate/jaap

# Comparative study of the effect of aluminum oleate in $CO_2$ and $N_2$ environments on the aquathermolysis of heavy oil

Yasser I.I. Abdelsalam [a,*], Elena A. Emelyanycheva [b], Lilia Kh. Galiakhmetova [a], Gadel F. Baimukhametov [a], Sergey A. Sitnov [a], Alexey V. Vakhin [a]

[a] Institute of Geology and Petroleum Technologies, Kazan Federal University, 18 Kremlyovskaya Str., Kazan 420008, Russia
[b] Department of Chemical Technology and Petroleum Refining, Kazan National Research Technical University, 10 K. Marx Str., Kazan 420111, Russia

ARTICLE INFO

*Keywords:*
Heavy oil
Viscosity reduction
Aquathermolysis
Oil-soluble catalyst
Aluminum oleate catalyst
$CO_2$
$N_2$

ABSTRACT

Oil-soluble catalysts present promising methods to enhance the efficiency of heavy oil extraction and processing. This study synthesized and characterized an oil-soluble aluminum oleate catalyst and conducted a comparative analysis of its catalytic efficiency in $CO_2$ and $N_2$ atmospheres for heavy oil processing via aquathermolysis at 300 °C for 24 hours. The results indicated that the reaction system in a $CO_2$ atmosphere exhibited, achieving a more substantial reduction in viscosity and asphaltene content compared to the $N_2$ atmosphere. The upgrading process also improved the H/C ratio and reduced sulfur content, highlighting the effectiveness of aromatization and desulfurization reactions. Infrared spectral analysis data revealed an increase in the (C═C/$CH_3$+$CH_2$) ratio and a decrease in the ($CH_2$/C═C) and ($RSO_3H$/C═C) ratios compared to heavy oil. These findings open new avenues for developing heavy oil processing technologies using aquathermolysis in the presence of aluminum oleate, significantly enhancing the efficiency of the upgrading process.

## 1. Introduction

The upgrading of heavy oil is one of the key tasks of the modern oil industry aimed at meeting the growing energy needs. Heavy oil is characterized by high density and viscosity, as well as the presence of heteroatoms such as sulfur, nitrogen, and oxygen, which significantly complicates its development and processing [1]. Thermal extraction methods are widely used for the effective exploitation of heavy oil fields, which allow for reducing the viscosity of oil and improving its flowability in reservoirs [2,3]. The steam injection process, which involves the continuous and cyclic introduction of hot liquid into oil reservoirs, facilitates the heating of the oil-bearing layer, which in turn reduces viscosity and improves the mobility of heavy oil [4]. However, despite the widespread use of this method, it faces a number of limitations. The main issues include low efficiency in complex geological formations, high energy costs for steam production, significant water consumption, and carbon emissions caused by the combustion of fossil fuels [5,6].

In response to these challenges, alternative approaches are being explored, with aquathermolysis emerging as a promising technology. This method offers the potential for more efficient utilization of thermal energy and reagents in the decomposition of heavy hydrocarbons, which can lead to reduced oil viscosity and improved flowability. The incorporation of $CO_2$ or $N_2$ in aquathermolysis represents a promising avenue for enhancing heavy oil processing efficiency. Introducing $CO_2$ into the process helps reduce the viscosity of heavy oil by swelling the oil matrix, thereby improving the mobility of hydrocarbons and increasing recovery rates [7–9]. Moreover, Anne-Christine et al. conducted a study evaluating the environmental consequences and benefits of $CO_2$ storage in active oil reservoirs, focusing on a site in Texas. It was found that the reservoir has a large capacity for $CO_2$ storage, and emissions from the process are minimal. Enhanced oil recovery (EOR) activities are virtually carbon-neutral when comparing the net storage potential to gasoline emissions from the additional oil extracted [10]. It's known that employing an inert $N_2$ atmosphere prevents undesirable oxidative reactions and stabilizes process parameters. The combined injection of nitrogen and steam can further enhance the efficiency of steam distillation by lowering steam pressure and facilitating the maintenance of higher temperatures [11,12].

Lee et al. observed a 7–25 % increase in oil production when using $CO_2$ as a carrier gas compared to $N_2$ under similar testing conditions [13]. Similarly, Masri found that retorting Jordan oil shale under $CO_2$ yielded a slightly higher oil output (31.65 gal/ton) than under $N_2$

* Corresponding author.
*E-mail address:* Sailor-ya@mail.ru (Y.I.I. Abdelsalam).

https://doi.org/10.1016/j.jaap.2025.107151
Received 27 January 2025; Received in revised form 30 March 2025; Accepted 24 April 2025
Available online 10 May 2025

**Table 1**
Characteristics of the heavy oil utilized.

| Parameter | Viscosity mPa·s, 20 °C | Elemental content (%) | | | | | SARA fractions (%) | | | |
|---|---|---|---|---|---|---|---|---|---|---|
| | | C | H | N | S | O | Saturates | Aromatics | Resins | Asphaltenes |
| **Error ( ± wt%)** | 1 | 0.5 | 0.5 | 0.03 | 0.2 | 0.05 | 0.3 | 0.5 | 0.4 | 0.2 |
| | 4000 | 81.98 | 11.12 | 0.38 | 5.54 | 0.98 | 25.6 | 32.3 | 34.5 | 7.6 |

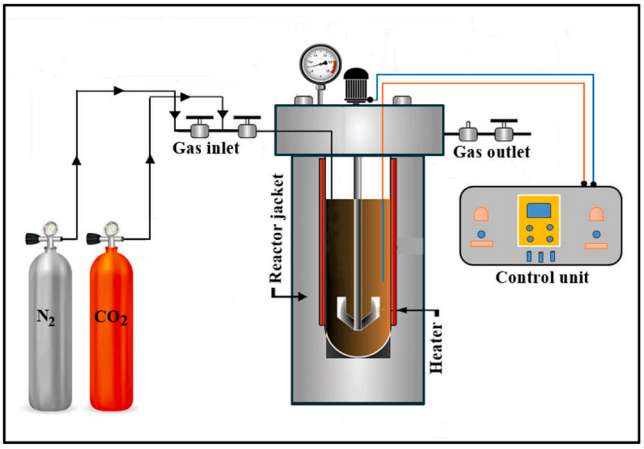


**Fig. 1.** Schematic diagram of a laboratory high-pressure batch autoclave.

(30.8 gal/ton), with a greater proportion of shorter-chain aliphatic hydrocarbons [14].

The application of oil-soluble catalysts in aquathermolysis is of particular interest. Such catalysts increase the selectivity and efficiency of the decomposition of complex hydrocarbon molecules, contribute to the reduction of viscosity, and increase the content of lighter and more valuable components. In this area, work was conducted by Yun-Rui Li and co-authors, which revealed the high efficiency of oil-soluble iron oleate catalysts in the process of heavy oil cracking. The studies demonstrated a viscosity reduction of 86.1 % during aquathermolysis at a temperature of 200 °C for 24 hours [15]. Furthermore, the work of N. N. Petrukhina et al. using an oil-soluble catalyst based on Ni, Co carboxylates combined with tetralin in the aquathermolysis process at 300 °C for 5 hours shows a viscosity reduction of 98 %. A composite catalyst containing 0.2 % copper aromatic sulfonate was used to heat heavy bitumen oil at 280 °C for 24 hours. It was noted that the viscosity of the heavy oil decreased by 95.5 % [16]. Vakhin et al. demonstrated that catalytic aquathermolysis using nickel tallate on oil-saturated crushed core samples at 300°C increased saturated hydrocarbon concentration while decreasing resin and asphaltene content [17].

Recent studies have enhanced the process of upgrading heavy oil using various methods, including composite catalysts based on transition metal salts and alkalis. Zhou et al. demonstrated that adding NaOH to $CuSO_4$ reduces oil viscosity by 81.43 % at 300 °C, improving catalytic activity through the formation of Cu and $CuO_x$ [18]. Aluminum catalysts also exhibit properties that inhibit the formation of undesirable by-products, making them particularly promising for aquathermolysis of heavy oil. Specifically, Yasser et al. investigated nano catalysts Al $(H_2PO_4)_3$ at 250 °C in a $N_2$ gas environment, demonstrating a substantial increase in heavy oil thermolysis efficiency, with the yield of the fraction boiling below 200 °C nearly tripling compared to the initial sample and exceeding the control variant by over 50 % [19]. Research by Ronal de la Cruz Parejas and co-authors indicated a viscosity reduction in the aquathermolysis of heavy oil by 12.9 % using $Al_2O_3$-NiO and by 13.4 % using $TiO_2$ at 250 °C over 12 hours, confirming the variety of catalysts capable of influencing the viscosity of heavy oils [20].

Despite extensive research in the field of deep processing of heavy crude oil, the creation of an effective technology for converting it into light distillates remains a relevant task. Aluminum-based catalysts play a key role in the processing of heavy crude oil due to their acidic properties, facilitating the carbon-ion mechanism reactions necessary for the hydrogenation and isomerization of heavy hydrocarbon fractions, as well as ensuring the thermal stability of the process [21]. Although numerous studies have been conducted on various metal oleates, an analysis of the existing literature indicates a lack of attention to the characteristics and potential of aluminum oleate as an independent catalyst.

The innovativeness of this research lies in the synthesis and application of oil-soluble catalysts based on aluminum oleate, which ensure uniform distribution throughout the volume of heavy oil during the aquathermolysis process. Upon heating and exposure to water, aluminum oleate hydrolyzes, leading to the formation of active nanoparticles $Al_xO_y$/AlOH. These nanoparticles are evenly dispersed in the oil phase, which contributes to an increase in the catalytic activity of the system by enhancing the surface area and the number of active sites. The experimental conditions under which aluminum oleate interacts with 10 g of water and gases $CO_2$ and $N_2$ at a pressure of 40 bar and a temperature of 300 °C are unique and have not been previously considered in the literature. These conditions also highlight the novelty of our approach and could significantly enhance the efficiency of heavy oil processing.

The aim of the study is to assess the impact of aluminum oleate on the aqueous thermolysis of heavy oil in $CO_2$ and $N_2$ atmospheres to determine optimal conditions that promote viscosity reduction and increase the yield of light distillates. To achieve this goal, methods such as infrared spectroscopy, elemental analysis, gas chromatography, and other analytical techniques will be used.

## 2. Experimental section

### 2.1. Preparation of oil-soluble catalysts (aluminum oleate)

Aluminum oleate was synthesized by mixing 10 mmol of aluminum sulfate [$Al_2(SO_4)_3 \cdot 18\ H_2O$] with 20 mmol of oleic acid ($C_{17}H_{33}COOH$). The oleic acid was dissolved in ethanol and stirred for 20 minutes. Then, NaOH was added to achieve a pH of 9, and sodium oleate ($C_{17}H_{33}COONa$) was slowly combined over 5 minutes. The resulting aluminum oleate was filtered, washed with ethanol, and dried at 30 °C.

**1- $C_{17}H_{33}COOH + NaOH \rightarrow C_{17}H_{33}COONa + H_2O$**

**2- $Al_2(SO_4)_3 + 3\ C_{17}H_{33}COONa \rightarrow 2Al(C_{17}H_{33}COO)_3 + 3Na_2SO_4$**

### 2.2. Catalytic aquathermolysis reaction of heavy oil

#### 2.2.1. Materials and methods

We employed a sample of heavy oil obtained from the Ashal'cha oil field situated in the Tatarstan Republic of Russia. The characteristics of the heavy oil, along with analysis errors for various parameters, are outlined in Table 1.

#### 2.2.2. Experimental setup and condition

A laboratory experiment was conducted to study the effect of an oil-soluble catalyst, aluminum oleate, in $CO_2$ and $N_2$ atmospheres on the catalytic aquathermolysis of heavy oil. The experiment was performed in a 300-mL high-pressure stainless steel HP/HT 4560 reactor (Parr USA; Fig. 1). The reaction mixture was prepared by mixing 50 g of heavy oil,

**Table 2**
Codes of samples.

| Sample | Code |
|---|---|
| Heavy oil | Heavy oil |
| Heavy oil+$H_2O$+$N_2$ | Blank-$N_2$ |
| Heavy oil+$H_2O$+$CO_2$ | Blank-$CO_2$ |
| Heavy oil+Tetralin+$H_2O$+$N_2$ | HT-$N_2$ |
| Heavy oil+ Tetralin+$H_2O$+ $CO_2$ | HT-$CO_2$ |
| Heavy oil+ Aluminum oleate+ Tetralin+$H_2O$+$N_2$ | H(AL)T-$N_2$ |
| Heavy oil+ Aluminum oleate+ Tetralin+$H_2O$+ $CO_2$ | H(AL)T-$CO_2$ |

10 g of distilled water, and 1 g of aluminum oleate, dissolved in tetralin (in a 1:1 ratio) at an atmospheric pressure of 40 bar. The reactor was then sealed and purged with $CO_2$ or $N_2$ for 10 minutes to remove air. Next, $CO_2$ or $N_2$ was introduced into the autoclave to achieve an initial pressure of 40 bar, and the mixture was heated to 300°C for 24 hours, resulting in a final pressure of 80–110 bar. After that, the product mixture was cooled to 25 °C to stop the reaction.

Table 2 presents data from experiments on non-catalytic and catalytic aquathermolysis in an atmosphere of $CO_2$ and $N_2$.

### 2.3. Analytical procedures

#### 2.3.1. FTIR spectroscopy

To analyze the structural composition of oil, including resins and asphaltenes extracted before and after treatment, Fourier FT-IR spectroscopy was performed using a Bruker Tensor II FTIR instrument, achieving a resolution of 4 cm1 over a wavelength range of 400–4000 $cm^{-1}$.

#### 2.3.2. Thermogravimetric analysis

The thermal stability of the synthesized R-PPG surfactant was assessed using a Netzsch STA 449 F1 Jupiter simultaneous thermal analyzer (30–600 °C, 5 °C/min heating rate, 50 mL/min airflow). Thermogravimetric (TG) data were analyzed using NETZSCH Proteus Analysis v5.2.1 and Kinetics Neo 2.1.2.2 software.

#### 2.3.3. X-ray diffraction analysis

The catalyst was characterized by X-ray diffraction (XRD) using a Shimadzu XRD-7000S diffractometer (Cu Kα radiation, 40 kV, 40 mA, 5°/min scan rate, 5–100° 2θ).

#### 2.3.4. SEM and EDX analysis

A Carl Zeiss Merlin field emission scanning electron microscope (FE-SEM) equipped with an Oxford Instruments Aztec X-Max energy dispersive X-ray (EDX) spectrometer (127 eV resolution) was used for analysis (9 mm working distance, 20 kV accelerating voltage).

#### 2.3.5. Ultimate analysis

The elemental composition of the heavy oils, both before and after upgrading, was analyzed using the Perkin Elmer 2400 Series II analyzer (Perkin Elmer, MA, USA). This instrument enables the measurement of carbon, hydrogen, nitrogen, oxygen, and sulfur content in the oil.

#### 2.3.6. SARA-analysis

Heavy oil composition was determined using SARA analysis (GOST 32269–2013 and ASTM D 4124–09). Asphaltenes were precipitated from 1.0 g of oil using 40 volumes of n-hexane. Maltenes were separated into saturated hydrocarbons, aromatic hydrocarbons, and resins using a chromatographic column packed with neutral alumina (calcined at 450 °C for 3 h).

#### 2.3.7. Viscosity measurements

Viscosity measurements (20–80 °C, 10 °C increments) of the initial and hydrothermally treated oils (with and without chemical agents) were performed using a FUNGILAB Alpha L rotational viscometer (TL5 spindle, 6.7 mL sample) equipped with a HUBER MPC K6 thermostat. Shear rate was calculated as 1.32 *RPM (manual). RPM was adjusted for temperature and torque (50–90 %). The viscometer exhibited a relative error of ± 1.0 % and high reproducibility (<0.2 % deviation).

#### 2.3.8. Atmospheric distillation

Atmospheric distillation of crude oil and its processed products was carried out at the ARH-LAB-03 unit (max. 400°C, 220 V, 750 W), which consists of a heater and a condenser.

#### 2.3.9. Proton nuclear magnetic resonance

$^1$H NMR spectra were acquired using a Bruker Avance 400 spectrometer (400.1 MHz, $CDCl_3$ solvent) and FTIR spectra using a Bruker Tensor spectrometer (KBr plates).

#### 2.3.10. Gas chromatography-mass spectrometry (GC-MS)

The saturated and aromatic hydrocarbon fractions in heavy oil samples (both before and after aquathermolysis) were examined using GC/MS (Chromatek-Crystal 5000.2) equipped with a mass spectrometric detector (214.2.840.083–10 with an ADVIS ion source). Data processing was performed on total ion current as well as ions with *m/z* 57, which correspond to normal and iso-alkanes. For the analysis of aromatic hydrocarbons, total ion current (TIC) data included the recording of ions at *m/z* 91, 105, 119, and 133 for alkylbenzenes and at *m/z* 128, 142, 156, 170, and 184 for naphthalenes, in addition to *m/z* 178, 192, 206, and 220 for phenanthrenes. Used a CR-5ms capillary column: 30 m × 0.25 mm ID, 0.25 μm film thickness, with helium as the carrier gas. The temperature program was linear (100–150 °C at 12.5 °C/min; 150–310 °C at 3 °C/min), followed by an 8-min isothermal hold at 300 °C. MS conditions: 70 eV ionization energy, 270 °C ion source temperature, 50–500 Da scan range (1 scan/s, unit resolution). Hydrocarbon identification utilized NIST library and literature data.

#### 2.3.11. Experimental safety protocols

The experiments were carried out in the HP/HT 4560 reactor (Parr USA), which has a capacity of 138 bar and 500°C, with the implementation of the following safety protocols:

*2.3.11.1. System integrity checks.* - Initial leak tests utilizing nitrogen gas at the operating pressure (maintained for 30 minutes with a permissible pressure ≤ loss of no more than 1 bar per hour).

*2.3.11.2. Safety mechanisms.* -The automatic safety relief valve is designed to operate at 110 % of the normal operating pressure.

-Activation of an emergency temperature shutdown (occurs through). thermocouple trigger.

-Continuous pressure monitoring (utilizing both electronic and mechanical). detection devices.

3- Carbon Dioxide Handling Procedures

- Controlled pressure increase with real-time monitoring
- Protocols for gradual filling (at a rate of less than 5 bar/min).

*2.3.11.3. Operator protection.* - Control and operation of equipment from a distant laboratory facility.

- Polycarbonate protective barriers
- Protective gloves designed for high-temperature applications (capable of withstanding temperatures of up to 600 °C) and safety eyewear.

*2.3.11.4. Emergency protocols.* - Automatic system shutdown in response to abnormal pressure conditions.

- Provision of controlled airflow via the exhaust system.
- Emergency evacuation protocols

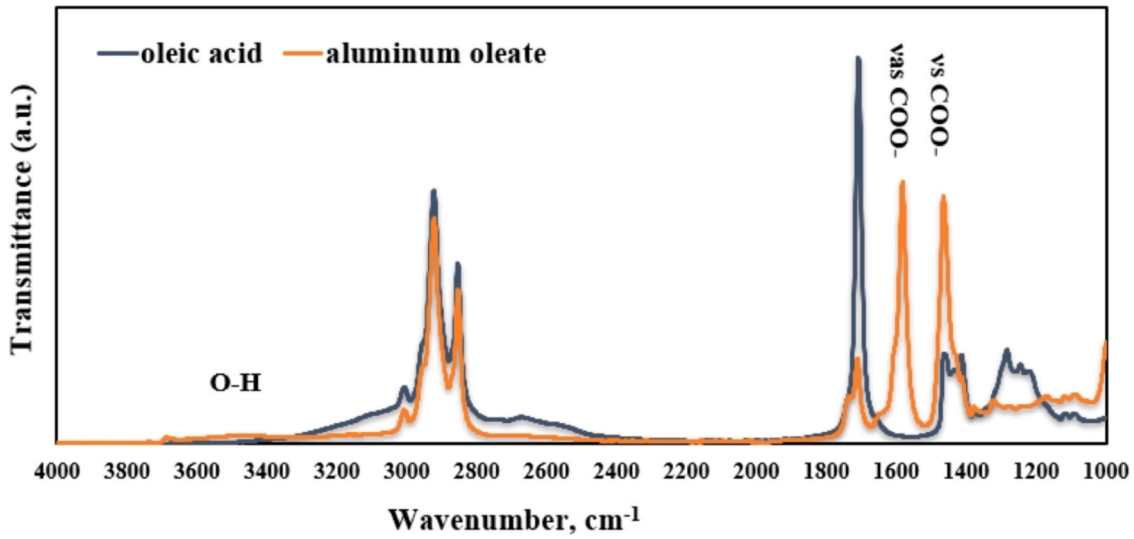


**Fig. 2.** FT-IR spectra of aluminum oleate and oleic acid.

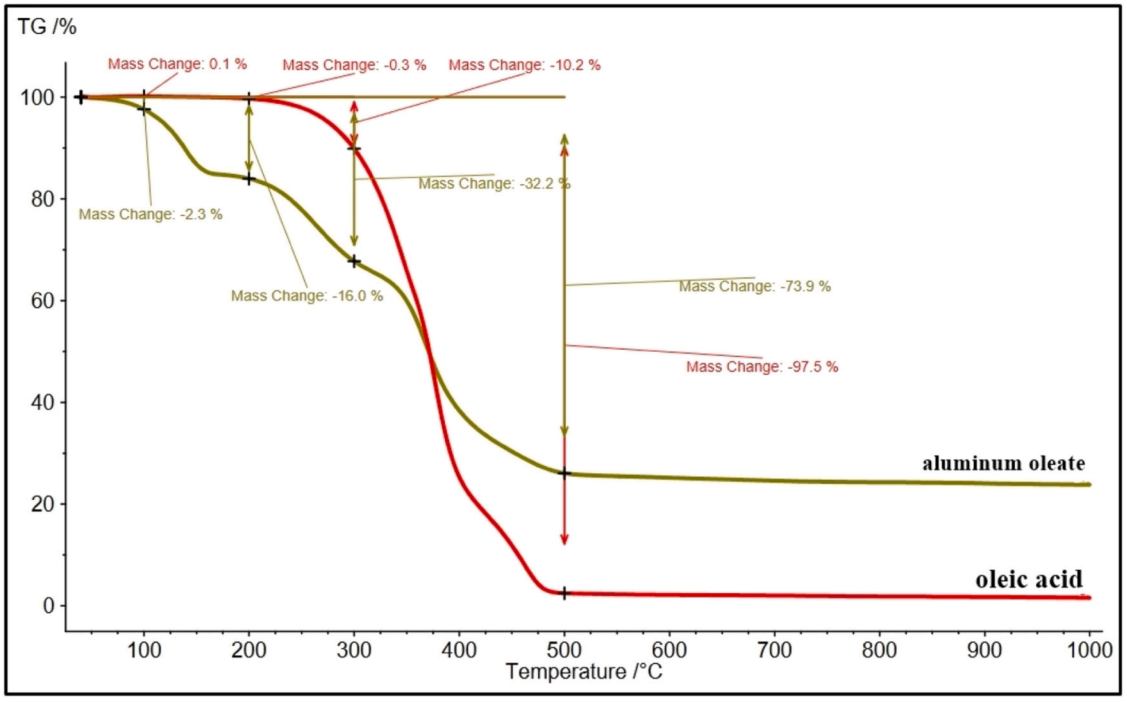


**Fig. 3.** TGA curves of aluminum oleate and oleic acid.

## 3. Results and discussion

### *3.1. Characterization of aluminum oleate (FT-IR, TGA, XRD, SEM and EDX)*

FT-IR spectra of oleic acid and aluminum oleate are shown Fig. 2. In the spectral analysis, two peaks emerged at 2920 and 2855 $cm^{-1}$, representing the symmetrical and asymmetrical –CH2 stretching modes. Another minor peak appeared at 3011 $cm^{-1}$, corresponding to the ν(C-H) of the C-H bond adjacent to the cis C═C bond. Additionally, a faint shoulder was observed at 2960 $cm^{-1}$, attributed to the asymmetrical –CH3 vibration mode. The broad signal spanning from 3500 to 2500 is indicative of the O–H stretching band of the acid, known to exist in a dimeric form due to hydrogen bonding. The prominent band at 1708 $cm^{-1}$ was linked to the ν(C═O) of the carboxyl group, signifying the presence of free oleic acid. A comparison of the spectra between aluminum oleate and pure oleic acid revealed two new peaks at 1584 $cm^{-1}$ and 1466 $cm^{-1}$, characteristic of the symmetric νs (COO −) and νas (COO −) stretch vibrations, respectively. These outcomes suggest that oleic acid chemisorbs onto the $Al_xO_y$ in the form of a carboxylate.

Fig. 3 illustrates the results of thermogravimetric analysis (TGA) of aluminum oleate and oleic acid, conducted in an argon atmosphere at a heating rate of 10 °C/min. The analysis showed significant differences in the thermal behavior of these substances.

At 40°C - 200 °C, aluminum oleate demonstrates a mass loss of 16 %, while oleic acid shows only 0.3 %, which is presumably due to the desorption of adsorbed moisture. Further heating to 300 °C leads to the dissociation of the oleate ligand in aluminum oleate and the formation of catalytically active centers, accompanied by a mass loss of 32.2 %.

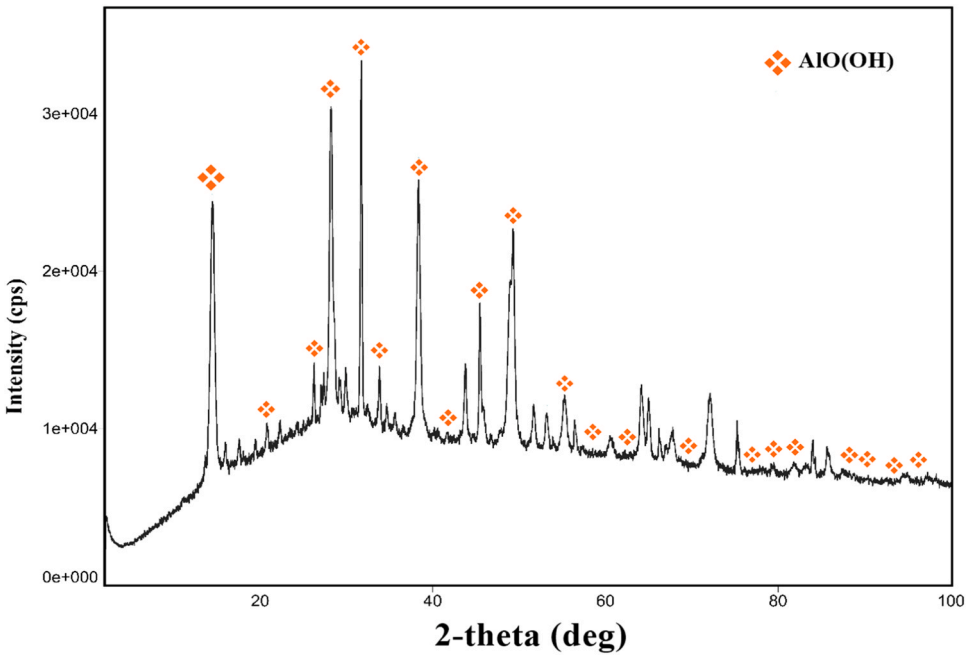


**Fig. 4.** XRD spectra of solid products improved to 300 °C after being separated from oil using aluminum oleate catalysts.

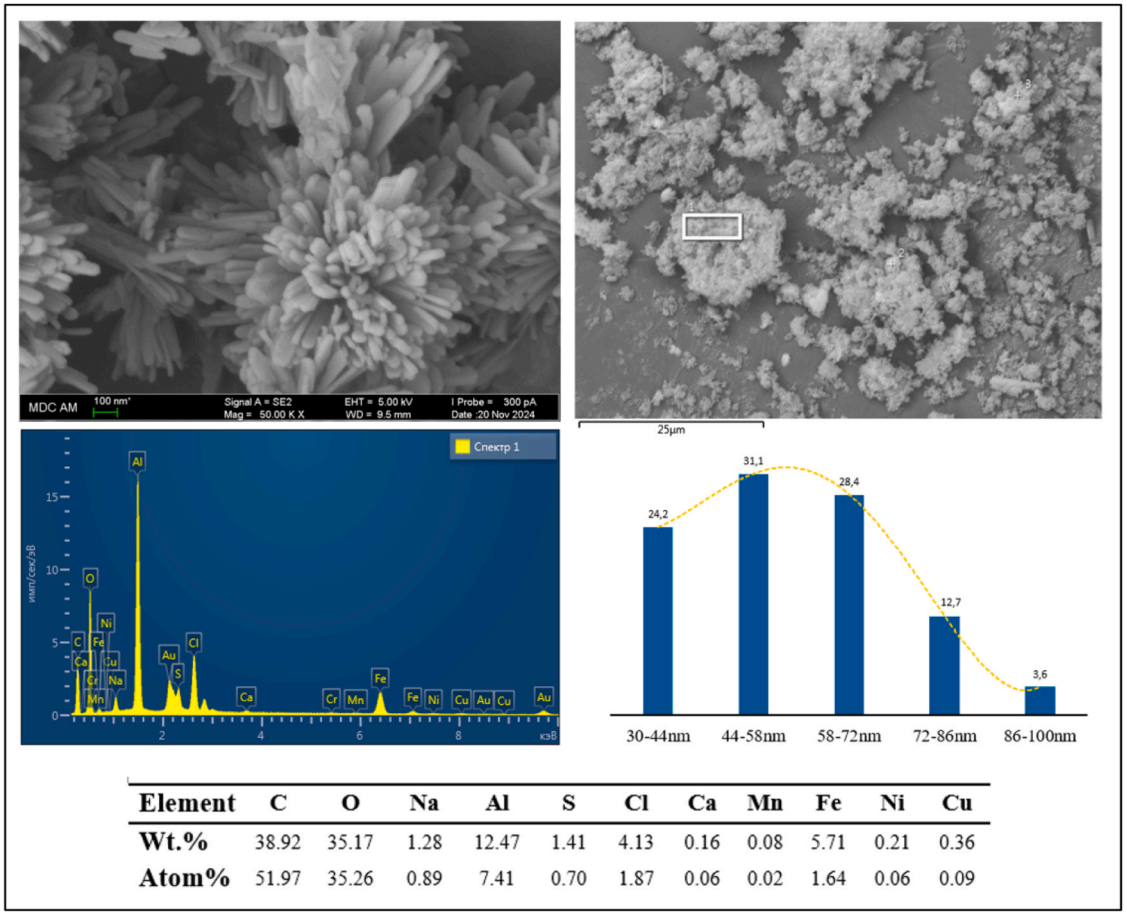


| Element | C | O | Na | Al | S | Cl | Ca | Mn | Fe | Ni | Cu |
|---|---|---|---|---|---|---|---|---|---|---|---|
| Wt.% | 38.92 | 35.17 | 1.28 | 12.47 | 1.41 | 4.13 | 0.16 | 0.08 | 5.71 | 0.21 | 0.36 |
| Atom% | 51.97 | 35.26 | 0.89 | 7.41 | 0.70 | 1.87 | 0.06 | 0.02 | 1.64 | 0.06 | 0.09 |

**Fig. 5.** SEM images (a, b), nanoparticle size frequency, and EDX analysis of aluminum oleate after aquathermolysis.

Under similar conditions, oleic acid loses 10.2 % of its mass.

At a temperature of 500 °C, the total mass loss is 73.9 % for aluminum oleate and 97.5 % for oleic acid. This indicates a significantly higher thermal stability of aluminum oleate compared to oleic acid. In the temperature range of 500–1000 °C, the mass of the samples remained virtually unchanged.

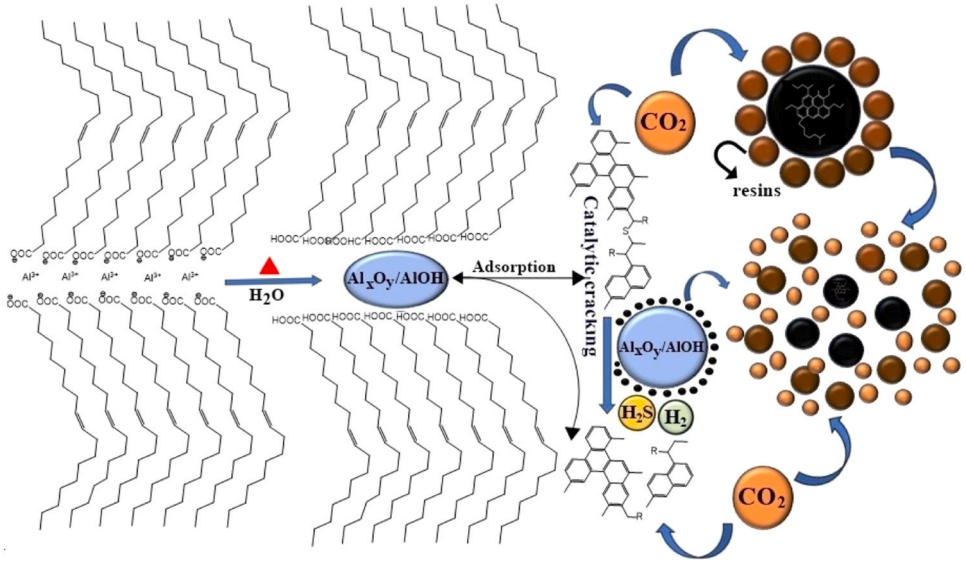


**Fig. 6.** Schematically presents the mechanism of catalytic aquathermolysis of heavy oil using aluminum oleate in a $CO_2$ atmosphere.

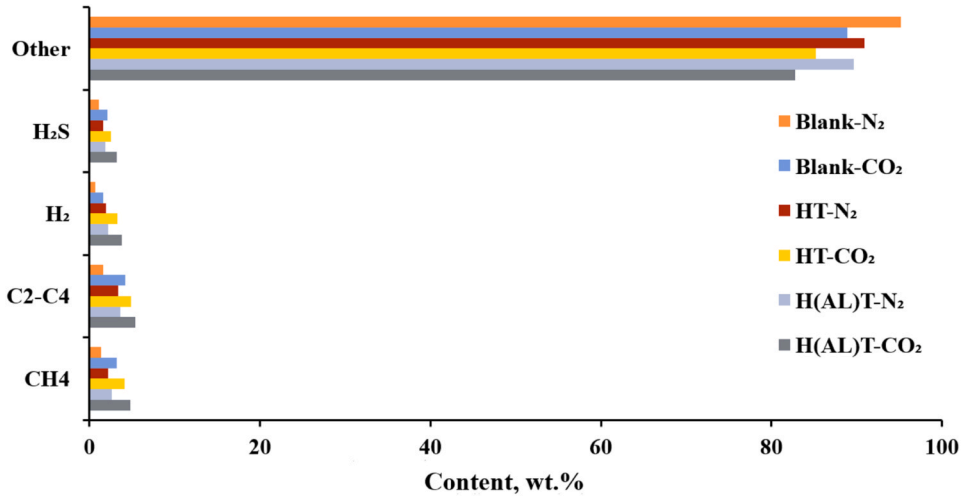


**Fig. 7.** Composition of the gas from the products of aquathermolysis conversion.

**Table 3**
Elemental composition of extra heavy oil and products of aquathermolysis.

| Samples | Elemental content (wt%) | | | | | |
|---|---|---|---|---|---|---|
| | C | H | S | N | O | H/C |
| **Heavy oil** | 81.98 | 11.12 | 5.54 | 0.38 | 0.98 | 1.63 |
| **Blank-$N_2$** | 82.14 | 12.1 | 4.58 | 0.33 | 0.85 | 1.77 |
| **Blank-$CO_2$** | 82.32 | 12.6 | 4.12 | 0.21 | 0.75 | 1.84 |
| **HT-$N_2$** | 82. 27 | 12.44 | 4.16 | 0.32 | 0.81 | 1.81 |
| **HT-$CO_2$** | 82.98 | 12.93 | 3.91 | 0.18 | 0.67 | 1.87 |
| **H(AL)T-$N_2$** | 82.28 | 12.59 | 4.14 | 0.22 | 0. 77 | 1.84 |
| **H(AL)T-$CO_2$** | 83.26 | 13.27 | 3.33 | 0.14 | 0. 56 | 1.91 |

The obtained data confirm the high thermal stability of aluminum oleate, making it a promising candidate for use as a catalyst in aquathermolysis processes.

The results of X-ray diffraction analysis (Fig. 4) demonstrate that the precursor of the aluminum oleate catalyst predominantly decomposes into AlO(OH) particles after catalytic cracking. Clear peaks corresponding to various crystal planes of AlO(OH) are observed in the diffraction patterns, which is confirmed by data from the JCPDS database (01–083–1505).

The surface morphology and elemental composition of the catalyst obtained after aquathermolysis were investigated using SEM and EDX, as illustrated in Fig. 5. The SEM analysis revealed that the particles possess an uneven and porous structure, which enhances the contact area between the catalyst and heavy oil, thereby improving catalytic activity. The EDX results confirmed the presence of aluminum and oxygen in the nanoparticles, consistent with the expected elemental composition of $Al_xO_y$ /AlOH.

Fig. 6 illustrates the combined effect of the oil-soluble catalyst (aluminum oleate) and $CO_2$ on the process of aquathermolysis. Under aquathermolysis conditions, aluminum oleate undergoes hydrolysis, forming active nanoparticles $Al_xO_y$/Al(OH), which are evenly dispersed in the oil phase. The mechanism of action of the catalyst $Al_xO_y$/Al(OH) is based on the adsorption and activation of hydrocarbon molecules through acidic centers located on the surface of nanoparticles. This process occurs via a radical chain mechanism that initiates a series of transformations, including dehydrogenation, hydrogenation, and isomerization. Furthermore, carbon dioxide ($CO_2$) serves as a heat carrier and solvent in the oil phase, facilitating the availability of reactive components for the catalyst. This, in turn, significantly enhances the efficiency

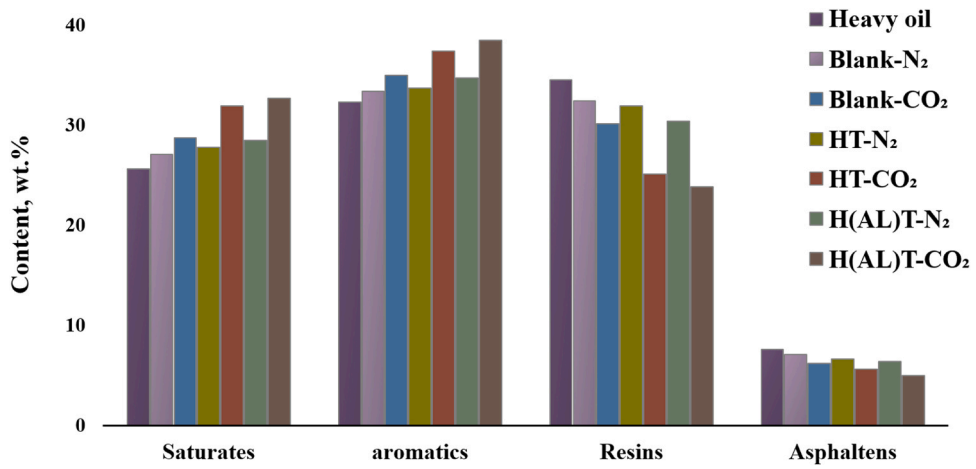


**Fig. 8.** Group composition of heavy oil and products of aquathermolysis.

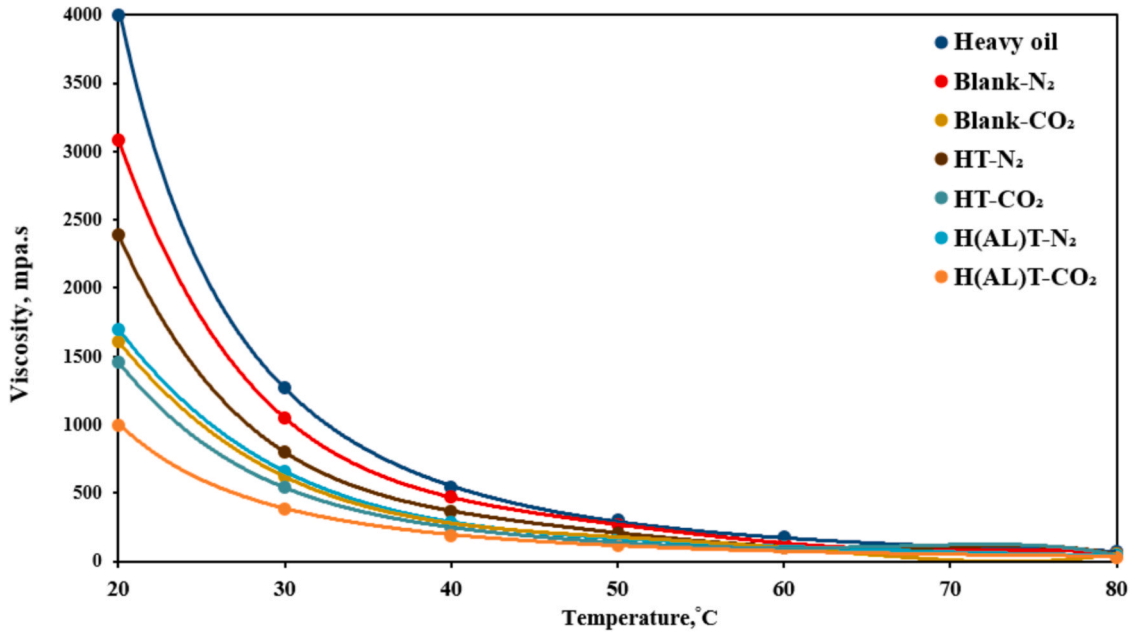


**Fig. 9.** Viscosity of heavy oil and products of aquathermolysis.

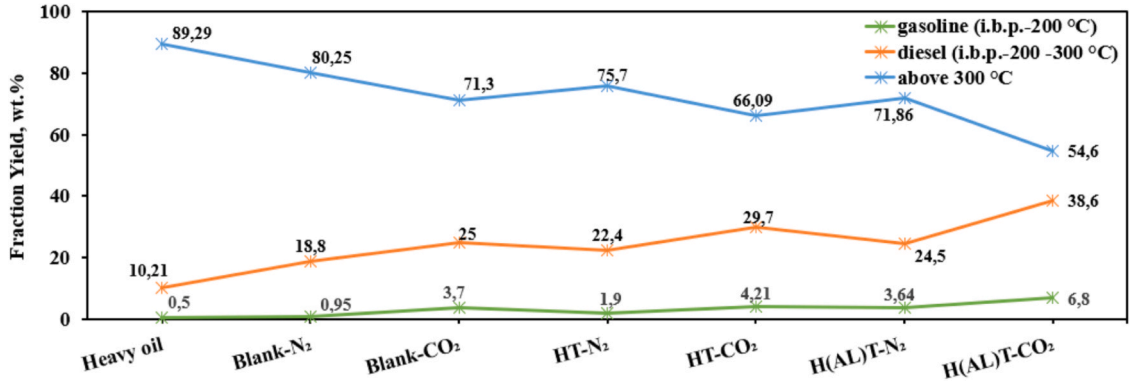


**Fig. 10.** Fractions of atmospheric distillation of heavy oil before and after aquathermolysis.

of the catalytic process by easing the cleavage of hydrocarbon chains containing C-heteroatoms and leads to the formation of lighter hydrocarbons as a result of hydrogenation. In contrast to carbon dioxide, nitrogen ($N_2$), being an inert gas, does not participate directly in chemical reactions; however, it is essential for maintaining pressure in the reaction system, which is necessary to achieve optimal conditions for

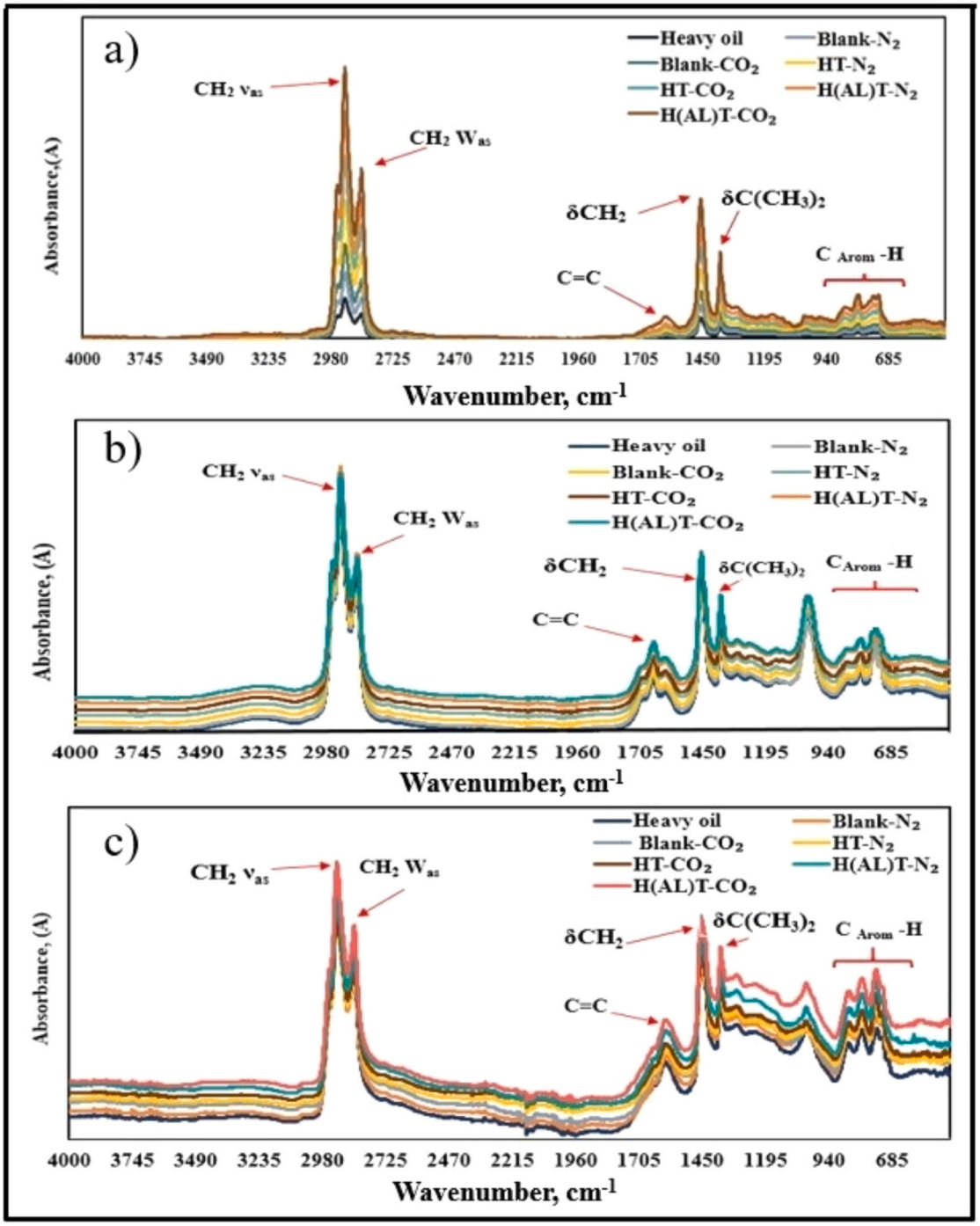


**Fig. 11.** IR spectra of heavy oil (a), resin (b), and asphaltene (c) fractions before and after aquathermolysis.

catalytic reactions.

Fig. 7 demonstrates the analysis of the gas composition, indicating the relationship between the concentrations of methane ($CH_4$), hydrocarbons $C_2$–$C_5$, and hydrogen sulfide ($H_2S$) with the experimental conditions. The increase in methane in the presence of $CO_2$ suggests a possible reduction reaction of $CO_2$ by hydrogen, leading to the formation of water and methane:

$CO_2 + 4H_2 \rightarrow CH_4 + 2\ H_2O$ [22]. Fluctuations in $H_2S$ concentration indicate the thermal decomposition of heavy hydrocarbons and their sulfur-containing components, which is more pronounced in the presence of $CO_2$ compared to $N_2$. This fact highlights the significant role of catalysts and $CO_2$ in catalytic cracking processes.

### 3.2. Elemental composition of heavy oil

Research has been conducted to study the changes in the elemental composition of heavy oil and the products of the aquathermolysis conversion reaction. The results of this study are presented in Table 3.

The aquathermolysis of heavy oil in $CO_2$ and $N_2$ environments was conducted both with and without the use of aluminum oleate as a catalyst. In both cases, a reduction in sulfur content was recorded: without a catalyst by 25.6 % (Blank-$CO_2$) and 17.3 % (Blank-N2) compared to the initial heavy oil, while with aluminum oleate by 40 % (H(AL)T-$CO_2$) and 25.3 % (H(AL)T-$N_2$) relative to the initial material. This indicates an effective breaking of the C–S bond under the influence of the catalyst and $CO_2$, which is due to specific interactions that lower

**Table 4**
Spectral FT–IR coefFicients of heavy oil, resin, and asphaltene fractions before and after aquathermolysis.

| Coefficient | Samples | CH2/C=C | C=C/CH3 +CH2 | CH3/CH2 | C=C/ CH3 | R-CO/ C=C | RSO3H/ C=C |
|---|---|---|---|---|---|---|---|
| Oil | Heavy oil | 8.10 | 0.15 | 1.80 | 0.27 | 0.43 | 1.31 |
| | Blank-$N_2$ | 6. 45 | 0.19 | 1.84 | 0.25 | 0.38 | 1.28 |
| | Blank-$CO_2$ | 7.69 | 0.31 | 1.89 | 0.17 | 0.25 | 1.18 |
| | HT-$N_2$ | 7.56 | 0.24 | 1.86 | 0.22 | 0.32 | 1.23 |
| | HT-$CO_2$ | 7.75 | 0.34 | 1.92 | 0.15 | 0.24 | 1.13 |
| | H(AL)T-$N_2$ | 7.62 | 0.28 | 1.91 | 0.19 | 0.29 | 1.2 |
| | H(AL)T-$CO_2$ | 7.84 | 0.36 | 1.95 | 0.13 | 0.20 | 1.0 |
| Resins | Heavy oil | 2.80 | 0.34 | 1.62 | 0.31 | 1.2 | 1.19 |
| | Blank-$N_2$ | 2.85 | 0.22 | 1.65 | 0.3 | 1.16 | 1.17 |
| | Blank-$CO_2$ | 2.96 | 0.29 | 1.75 | 0.28 | 0.96 | 1. 11 |
| | HT-$N_2$ | 2.89 | 0.24 | 1.67 | 0.27 | 1.11 | 1.15 |
| | HT-$CO_2$ | 3.0 | 0.3 | 1.78 | 0.25 | 0.92 | 1.04 |
| | H(AL)T-$N_2$ | 2.91 | 0.26 | 1.7 | 0.26 | 0.99 | 1.12 |
| | H(AL)T-$CO_2$ | 3.1 | 0.32 | 1.81 | 0.24 | 0.90 | 0.97 |
| Asphaltenes | Heavy oil | 1.38 | 0.37 | 1.2 | 0.44 | 1.71 | 1.27 |
| | Blank-$N_2$ | 1.23 | 0.39 | 1.23 | 0.37 | 1.67 | 1.25 |
| | Blank-$CO_2$ | 1.3 | 0.47 | 1.34 | 0.29 | 1.58 | 1.19 |
| | HT-$N_2$ | 1.26 | 0.41 | 1.27 | 0.33 | 1.64 | 1.23 |
| | HT-$CO_2$ | 1.33 | 0.54 | 1.37 | 0.25 | 1.44 | 1.17 |
| | H(AL)T-$N_2$ | 1.29 | 0.46 | 1.30 | 0.31 | 1.61 | 1.2 |
| | H(AL)T-$CO_2$ | 1.36 | 0.58 | 1.40 | 0.22 | 1.42 | 1.14 |

$CH_{2/C=C)}$ =D1450/D1600, aliphaticity. (C=C/CH3+CH2) = D1600/D720ю1380, aromaticity. CH3/CH2 = D1380/D720, branching. (C=C/ CH3)= D1600/D740ю860 degree of condensation. (R-C=O/ C=C) =D1700/D1600, degree of oxidation. (RSO3H/C=C) = D1030/D1600, degree of sulfurization.

**Table 5**
$^1$ H NMR analysis of the heavy oil and products of aquathermolysis.

| Samples | $H_{A,\ \%}$ | Hά, % | $H_{\beta,\ \%}$ | Hγ, % | $f_A$ | $H_{AU/CA}$ | BI | σ |
|---|---|---|---|---|---|---|---|---|
| **Heavy oil** | 16.95 | 13.28 | 41.81 | 27.96 | 0.324 | 1.185 | 0.338 | 0.281 |
| **Blank-$N_2$** | 13.78 | 13.63 | 44.56 | 28.03 | 0.238 | 1.530 | 0.321 | 0.331 |
| **Blank-$CO_2$** | 10.85 | 14.23 | 45.30 | 29.62 | 0.181 | 1.820 | 0.332 | 0.396 |
| **HT-$N_2$** | 12.57 | 13.79 | 44.75 | 28.89 | 0.207 | 1.708 | 0.329 | 0.354 |
| **HT-$CO_2$** | 8.15 | 14.45 | 47.03 | 30.37 | 0.141 | 2.035 | 0.329 | 0.470 |
| **H(AL)T-$N_2$** | 11.10 | 14.20 | 45.25 | 29.45 | 0.184 | 1.818 | 0.330 | 0.390 |
| **H(AL)T-$CO_2$** | 7.04 | 15.12 | 47.44 | 30.4 | 0.111 | 2.515 | 0.324 | 0.518 |

the activation energy for the reaction, facilitating the formation of active intermediate compounds and selective action on the molecules [23,24]. Moreover, in all conducted experiments, an increase in the atomic ratio of H/C was observed, reaching 1.91 (H(AL)T-$CO_2$) and 1.84 (H(AL)T-$N_2$) in the presence of aluminum oleate. This increase is associated with several factors: Carbon dioxide reduces the interfacial tension, improving the availability of reagents between the oil and the catalyst [25–27]. The interaction of $CO_2$ with $Al_xO_y$/AlOH modifies the active centers of the catalyst, enhancing its activity in hydrogenation, isomerization, and the breaking of C-heteroatom bonds, leading to the formation of more saturated hydrocarbons [28]. This effect is specific to the $CO_2$ environment and is less pronounced in the $N_2$ environment.

### 3.3. Group compositions analysis SARA

Fig. 8 shows that the Blank-$CO_2$ and Blank-$N_2$ samples demonstrate a significant reduction in resin content (12.8 % and 6.1 %) and asphaltenes (18.4 % and 6.6 %) compared to heavy oil. In the case of using aluminum oleate, the H(AL)T-$CO_2$ and H(AL)T-$N_2$ samples showed a more pronounced reduction in resins by 31 % and 11.9 %, respectively, as well as asphaltenes by 34.2 % and 15.8 % compared to heavy oil.

The reduction of resins and asphaltenes due to the aquathermolysis of heavy oil is attributed to several key mechanisms. The increased temperature and pressure during aquathermolysis enhance the thermochemical decomposition of heavy hydrocarbons [16]. Furthermore, the use of $CO_2$ aids in the liquefaction of asphaltenes and resins, increasing their solubility and facilitating the decomposition of heavy hydrocarbons [29,30]. This results in a transition from more complex structures of resins and asphaltenes to simpler molecular forms. Moreover, in a $CO_2$ environment, there is active interaction with $Al_xO_y$/AlOH, which enhances its catalytic activity and leads to effective cracking and dehydrogenation reactions [31]. These processes contribute to the degradation of resins and asphaltenes, ultimately resulting in a reduction of their concentration in the final products.

### 3.4. Viscosity analysis

The viscosity measurement results of heavy oil and products of catalytic aquathermolysis are shown in Fig. 9.

The viscosity of aquathermolysis products decreased proportionally based on the process conditions compared to the viscosity of heavy oil. The experimental conditions Blank-$CO_2$ and Blank-$N_2$ demonstrated viscosity reductions of 59 % and 23 %, respectively, at a temperature of 20 °C compared to heavy oil.The use of an aluminum oleate catalyst led to an even more significant viscosity reduction: in the samples H(AL)T-$CO_2$ and H(AL)T-$N_2$, viscosity reductions of 74.8 % and 57.5 %, respectively, were observed relative to the viscosity of heavy oil. These results indicate that the high solubility of $CO_2$ in the oil phase enhances interaction with heavy oil, which, in turn, facilitates deeper penetration into the structure of high molecular weight compounds [32]. On the contrary, Nitrogen ($N_2$) is an inert gas characterized by high heat capacity and the ability to create pressure. It is nearly insoluble and does not engage in chemical reactions with hydrocarbons [33]. Moreover, the acidic properties of $Al_xO_y$/Al(OH) promote the flow of reactions by the carbon-ionic mechanism, accelerating hydrogenation and isomerization reactions. This leads to the decomposition of large hydrocarbons into smaller and branched chains [15]. The interaction of $CO_2$ with $Al_xO_y$/AlOH also helps to loosen the molecular structure and reduce intermolecular forces, leading to the transformation of the normal structure of hydrocarbons into a branched form, thereby further

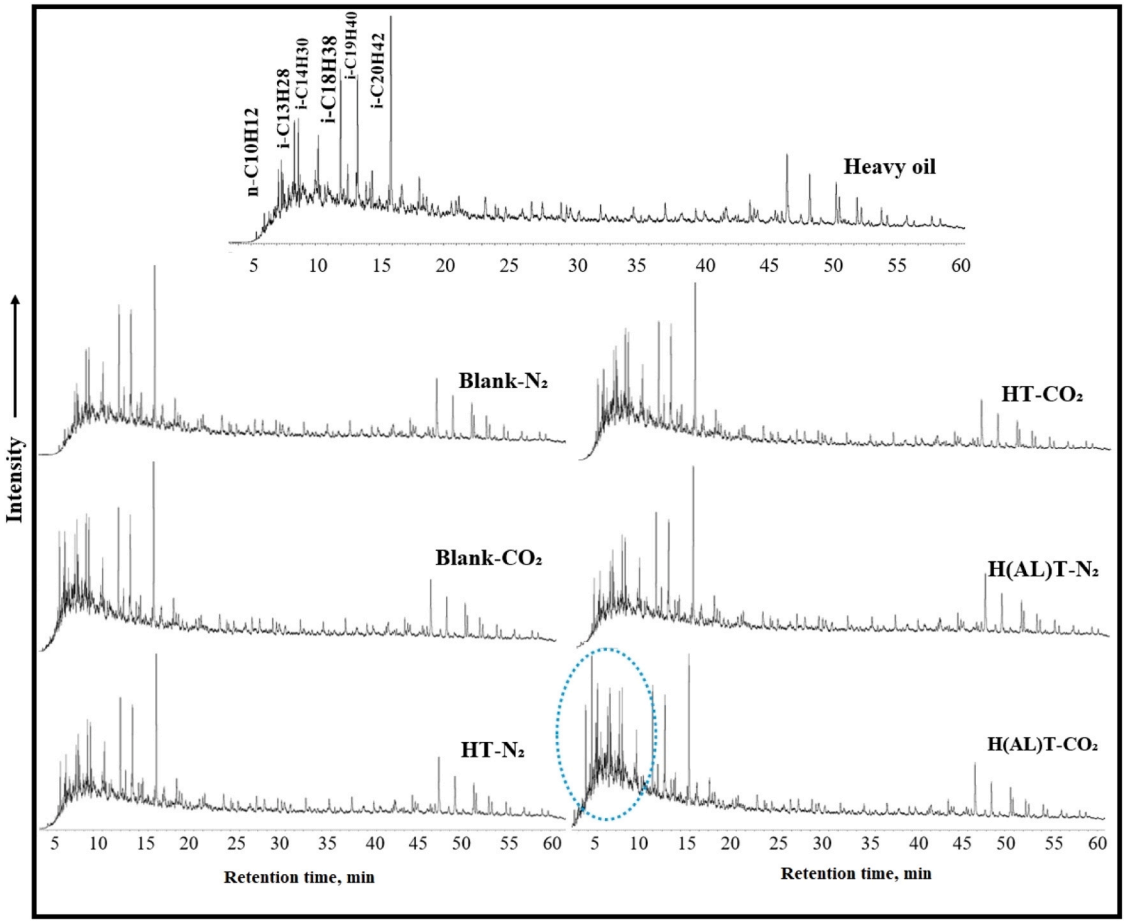


**Fig. 12.** The GC-MS spectra of saturated hydrocarbons before and after catalytic thermolysis.

decreasing the viscosity of heavy oil.

### 3.5. Atmospheric distillation of heavy oil

Fig. 10 demonstrates that both non-catalytic and catalytic aquathermolysis in a $CO_2$ environment, compared to $N_2$, results in a significantly higher share of light fractions, particularly gasoline (boiling point up to 200°C) and diesel fuel (200–300°C). The catalytic activity of aluminum oleate in the process of aquathermolysis contributed to a significant increase in the yield of light fractions (gasoline + diesel, boiling up to 300 °C). The initial yield of heavy oil, which was 10.72 %, increased to 46.4 % in the H(AL)T-$CO_2$ sample and to 28.24 % in the H(AL)T-$N_2$ sample. This is explained by the high potential of carbon dioxide ($CO_2$) for intermolecular interaction, and its contact with water ($H_2O$) leads to the formation of carbonic acid, which exhibits acidic properties. As a result, in an acidic environment, an ion ($H^+$) is formed, which participates in the chemical reaction mechanism of isomerization, thereby increasing the share of isomers.

$CO_2 + H_2O = H_2CO_3$ [34]

$H_2CO_3 \rightleftharpoons H^+ + HCO_3$- [35]

The addition of AlxOy/AlOH further increases the yield of light fractions and accelerates both hydrogenation and isomerization reactions. Consequently, this process enhances the quality characteristics of gasoline and diesel fractions obtained from heavy oil. In contrast, $N_2$ does not exhibit significant reactivity.

### 3.6. Analysis FTIR of aquathermolysis products

Fig. 11 shows that infrared spectroscopy (IR) of heavy oil (a), resin (b), and asphaltene (c) fractions before and after aquathermolysis demonstrates significant changes in the functional groups of oil samples in the range from 400 $cm^{-1}$ to 4000 $cm^{-1}$. These changes indicate the effectiveness of the process in improving the quality of heavy oil.

The data analysis in Table 4 compares the relative values of spectral coefficients for different groups.

The analysis of asphaltene fractions and heavy oil before and after aquathermolysis revealed a decrease in aliphaticity coefficients and an increase in aromaticity, caused by dehydrocyclization reactions and dehydrogenation of naphthenes leading to the formation of aromatic compounds (arenes) [36]. In contrast to asphaltenes, resins show an increase in aliphaticity and a decrease in aromaticity, which may be related to the hydrogenation of unsaturated compounds and the isomerization of aromatic structures into aliphatic ones [37]. The analysis of sulfur content, recalculated to sulfoxides (R-S(=O)-R), showed a more significant decrease in the presence of $Al_xO_y$/AlOH nanoparticles, which possess acidic centers and the ability to dissolve $CO_2$, creating conditions for increased catalytic activity. This, in turn, accelerates reactions and reduces the activation energy required to break C–S bonds. As a result, more efficient desulfurization of oil occurs, ultimately leading to its improvement [38,39].

### 3.7. Nuclear magnetic resonance

The 1H-NMR spectra examined heavy oil before and after aquathermolysis. The distribution of hydrogen atom types includes: HA-aromatic hydrogen (9.0–6.0 ppm), Hα-aliphatic hydrogen on Cα, adjacent to aromatic rings (4.0–2.0 ppm), Hβ-aliphatic hydrogen on Cβ and CH2, as well as CH for Cβ near aromatic rings (2.0–1.0 ppm), and Hγ-aliphatic hydrogen on Cγ and CH3 for Cγ, which is adjacent to aromatic rings (1.0–0.5 ppm). This classification was achieved using chemical

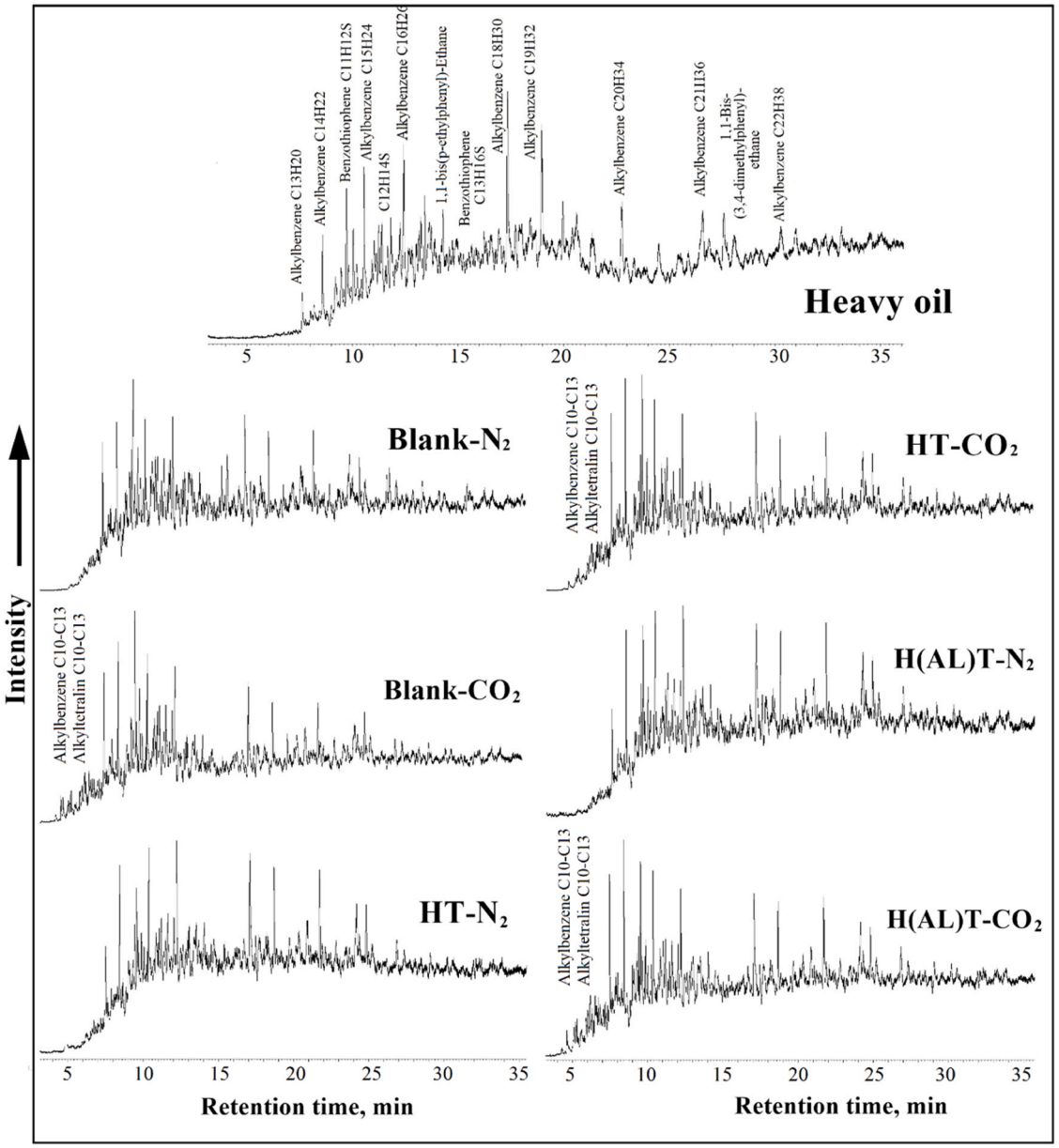


**Fig. 13.** The GC–MS spectra (TIC) of aromatics hydrocarbon fractions before and after catalytic thermolysis.

shifts and integral areas. Furthermore, structural parameters of the aromatic hydrocarbons were calculated, including aromaticity (fA), condensation aromaticity (HAU/CA), branching index (BI), and conversion rate in aromatic rings (σ), employing enhanced methods developed by Brown-Ladner.1–4 [40–42].

The results presented in Table 5 demonstrate that both in non-catalytic and catalytic aquathermolysis, there is a decrease in the level of aromaticity (fA) and an increase in the aromaticity condensation coefficient (HAU/CA). This indicates that aromatic compounds are being transformed into less aromatic or aliphatic structures, which contributes to the formation of more stable aromatic compounds with a reduced tendency for further decomposition. Moreover, the coefficient of aromaticity condensation (HAU/CA) of heavy oil products from aquathermolysis conversion in a CO2 environment is higher than in an N2 environment. This is because CO2 can promote better mixing and dissolution of aromatic hydrocarbons, which increases the condensation coefficient. At the same time, N2has a less pronounced effect on the condensation of aromatic compounds, leading to a lower coefficient in this environment. The decrease in the branching index (BI) indicates processes of dehydrogenation and dealkylation, leading to the removal of side alkyl chains from hydrocarbon molecules and, consequently, to a reduction in the number of branches in their structure. Thus, aquathermolysis not only leads to a change in the composition of hydrocarbons but also increases the stability of the resulting compounds [43].

### 3.8. Analysis of GC-MS spectra

Chromatographic analysis of fractions of saturated hydrocarbons extracted during the aquathermolysis of heavy oil (Fig. 12) shows dynamic changes in their composition. We observe that the peak maximum shifts to the left, indicating an increase in the relative content of low molecular weight n-alkanes and iso-alkanes. This phenomenon is associated with the breakdown of long-chain alkanes, leading to the formation of more volatile and short-chain homologues. Hydrogenation and aromatization reactions may also contribute to the observed changes. However, interactions with ($Al_xO_y$/AlOH) and CO2 promote more intense destruction of high molecular weight compounds, which is manifested in the increased intensity of n-alkane peaks with a retention

time of less than 10 minutes. This effect allows tracking the dynamics of changes in the composition of saturated hydrocarbons over time. At later stages of the chromatogram analysis, clear and intense peaks are preserved, which may indicate the stabilization of the hydrocarbon composition and the completion of key degradation processes.

Chromatographic analysis of the total ion current (TIC) of the aromatic fraction of heavy oil samples subjected to aquathermolysis (Fig. 13) shows significant changes in the composition of these fractions under the influence of catalytic treatment. In the initial stages of the study, peaks corresponding to alkylbenzenes (C10-C13) and tetralins are detected and recorded before the eighth minute of chromatographic analysis. The presence of a catalyst ($Al_xO_y$/AlOH) in the midst of $CO_2$ leads to significant modifications of the chromatographic profile of the samples. At the same time, a decrease in the intensity of peaks characteristic of alkylbenzenes and alkyltetralins is noted, along with the emergence of new peaks, indicating transformations in the composition of aromatic hydrocarbons. It has been established that in the sample treated with a catalyst and $CO_2$, a more pronounced transformation of low-boiling aromatic compounds is observed. At later stages of the process, a significant decrease in peak intensity is observed, which may indicate the deep transformation or destruction of most of the original compounds. At the same time, a greater diversity of peaks is recorded in the $CO_2$ environment compared to using $N_2$, which may indicate more complex reaction processes occurring under catalytic reaction conditions.

## 4. Conclusions

This work presents the mechanism of action of an oil-soluble catalyst based on aluminum oleate and $CO_2$ in the process of aquathermolysis. Under aquathermolysis conditions, aluminum oleate undergoes hydrolysis, forming active nanoparticles $Al_xO_y$/Al(OH), which are uniformly dispersed in the oil phase, catalyzing hydrogenation and isomerization reactions. Meanwhile, $CO_2$ acts as a heat carrier and solvent, which, in combination with the catalyst's action, enhances overall catalytic activity and facilitates more effective interaction with oil components, thereby improving its processing. The research results indicate that the use of aluminum oleate in the presence of $CO_2$ significantly increases the upgrading efficiency compared to the use of $N_2$. The interaction of $CO_2$ with aluminum oleate modifies the active centers of the catalyst, increasing its efficiency in dehydrogenation, hydrogenation, and breaking C-heteroatom bonds, leading to a significant increase in the H/C ratio (1.91), a reduction in viscosity (74.8 %), as well as a decrease in sulfur content (40 %) and asphaltenes (34.2 %) in oil samples compared to heavy oil. Additionally, the yield of light fractions (gasoline + diesel) increases to 300 °C from 10.72 % to 46.4 %, respectively. These results highlight the importance of selecting the medium for catalytic processes, opening new prospects for improving the efficiency of heavy oil processing. Further research should focus on optimizing process parameters and studying other catalysts and combined methods to enhance upgrading efficiency, including pilot and industrial tests.

## CRediT authorship contribution statement

**Alexey Vakhin:** Validation. **Elena A. Emelyanycheva:** Validation. **Yasser Abdelsalam:** Writing – review & editing, Writing – original draft, Visualization, Resources, Methodology, Investigation, Formal analysis, Data curation, Conceptualization. **Gadel Baimukhametov:** Validation. **Lilia Galiakhmetova:** Validation. **Sergey Sitnov:** Validation.

## Funding

This work was funded by the subsidy allocated to Kazan Federal University for the state assignment in the sphere of scientific activities, project N№ FZSM-2023-0014.

## Declaration of Competing Interest

The authors declare that they have no known competing financial interests or personal relationships that could have appeared to influence the work reported in this paper.

## Data availability

No data was used for the research described in the article.

## References

[1] H. Al-Awadi, Multiphase Characteristics of High Viscosity Oil, (2011).
[2] I.I. Mukhamatdinov, M.O.N. Ali, R.E. Mukhamatdinova, B. Affane, A.V. Vakhin, S. V. Tsvetkov, S.Y. Malaniy, A.N. Protsenko, Optimization of thermal steam treatment technology applied to Strelovskoye field using aquathermolysis catalysts, Fuel 359 (2024) 130389.
[3] T. Kholmurodov, A. Tajik, Y. Galyametdinov, R. Ksenia, S. Mehrabi-Kalajahi, O. Mirzaev, A.V. Vakhin, Mechanism of surfactant peptization in the process hydrocatalytic degradation of asphaltenes in heavy oils, Fuel 381 (2025) 133490.
[4] M.A. Yongsheng, C.A.I. Xunyu, L.I. Maowen, L.I. Huili, Z.H.U. Dongya, Q.I. U. Nansheng, P. Xiongqi, Z. Daqian, K. Zhijiang, M.A. Anlai, Research advances on the mechanisms of reservoir formation and hydrocarbon accumulation and the oil and gas development methods of deep and ultra-deep marine carbonates, Pet. Explor. Dev. 51 (2024) 795–812.
[5] A.M.A. Hasan, R.S. Kamal, R.K. Farag, M.E. Abdel-Raouf, Petroleum sludge formation and its treatment methodologies: a review, Environ. Sci. Pollut. Res. 31 (2024) 8369–8386.
[6] A.H. Ikevuje, J.M. Kwakye, D.E. Ekechukwu, O.B. Ogundipe, A.E. Esiri, Negative crude oil prices: Supply chain disruptions and strategic lessons, J. Multidiscip. Stud. 8 (2024) 85–93.
[7] S. Davoodi, M. Al-Shargabi, D.A. Wood, M. Mehrad, V.S. Rukavishnikov, Carbon dioxide sequestration through enhanced oil recovery: a review of storage mechanisms and technological applications, Fuel 366 (2024) 131313.
[8] P. Fang, Q. Zhang, C. Zhou, Z. Yang, H. Yu, M. Du, X. Chen, Y. Song, S. Wang, Y. Gao, Chemical-assisted CO2 water-alternating-gas injection for enhanced sweep efficiency in CO2-EOR, Molecules 29 (2024) 3978.
[9] P. Wei, W. Pu, L. Sun, Y. Pu, S. Wang, Z. Fang, Oil recovery enhancement in low permeable and severe heterogeneous oil reservoirs via gas and foam flooding, J. Pet. Sci. Eng. 163 (2018) 340–348.
[10] A.-C. Aycaguer, M. Lev-On, A.M. Winer, Reducing carbon dioxide emissions with enhanced oil recovery projects: a life cycle assessment approach, Energy Fuels 15 (2001) 303–308.
[11] Z. Lin, X. Lu, X. Wang, Y. Chang, K. Kang, F. Zeng, Effect of N2 impurity on CO2-based cyclic solvent injection process in enhancing heavy oil recovery and CO2 storage, Energy 290 (2024) 130227.
[12] J. Zhao, Y. He, J. Wang, M. Peng, J. Yang, F. Zeng, Effect of in-situ emulsification on CO2/N2-based cyclic solvent injection process for enhancing heavy oil recovery and CO2 storage, Chem. Eng. Sci. 295 (2024) 120185.
[13] S. Lee, R. Joshi, Enhanced Oil Recovery From Western United States Type Oil Shale Using Carbon Dioxide Retorting Technique, 1985.
[14] B.J. Masri, Extraction and Characterization of the El-lajun Jordan Oil Shale, (1998).
[15] Y.-R. Li, Q.-Y. Li, X.-D. Wang, L.-G. Yu, J.-J. Yang, Aquathermolysis of heavy crude oil with ferric oleate catalyst, Pet. Sci. 15 (2018) 613–624.
[16] N.N. Petrukhina, G.P. Kayukova, G.V. Romanov, B.P. Tumanyan, L.E. Foss, I. P. Kosachev, R.Z. Musin, A.I. Ramazanova, A.V. Vakhin, Conversion processes for high-viscosity heavy crude oil in catalytic and noncatalytic aquathermolysis, Chem. Technol. Fuels Oils 50 (2014) 315–326.
[17] A.V. Vakhin, F.A. Aliev, I.I. Mukhamatdinov, S.A. Sitnov, S.I. Kudryashov, I. S. Afanasiev, O.V. Petrashov, D.K. Nurgaliev, Extra-heavy oil aquathermolysis using nickel-based catalyst: some aspects of in-situ transformation of catalyst precursor, Catalysts 11 (2021) 189.
[18] Y. Zhou, Q. Zhao, Y. Miao, X. Wang, Y. Zhang, Y. Wang, L. Guo, Study on the synergistic effect of NaOH and CuSO4 in aquathermolysis upgrading, Fuel Process. Technol. 244 (2023) 107715.
[19] Y.I.I. Abdelsalam, R.F. Khamidullin, V.E. Katnov, A.V. Dengaev, F.A. Aliev, A.V. Vakhin, Influence of FeP and Al (H2PO4) 3 Nanocatalysts on the Thermolysis of Heavy Oil in N2 Medium, Catalysts 13 (2023) 390.
[20] R. de la Cruz Parejas, F.J. Moura, R.R. de Avillez, P.R. de Souza Mendes, Effects of Al2O3-NiO, TiO2 and (Mg, Ni) O particles on the viscosity of heavy oil during aquathermolysis, Colloids Surfaces A Physicochem, Eng. Asp. 625 (2021) 126863.
[21] M.R. Mason, Aluminum-Based Catalysis, John Wiley & Sons, Ltd: New York, 2015.
[22] N. Bespalko, A.-C. Roger, J. Bussi, Comparative study of NiLaZr and CoLaZr catalysts for hydrogen production by ethanol steam reforming: Effect of CO2 injection to the gas reactants. Evidence of Rh role as a promoter, Appl. Catal. A Gen. 407 (2011) 204–210.
[23] M. Breysse, E. Furimsky, S. Kasztelan, M. Lacroix, G. Perot, Hydrogen activation by transition metal sulfides, Catal. Rev. 44 (2002) 651–735.
[24] T. Ganguly, A.B. Chakraborty, A. Majumdar, Transition metal mediated hydrolysis of C–S bonds: an overview of a new reaction strategy, ACS Org. Inorg. Au 3 (2023) 332–349.

[25] Z. Chen, Y. Dong, H. Hu, X. Zhang, S. Tang, Evaluation of the synergistic oil displacement effect of a CO2 low interfacial tension viscosity-increasing system in ultra-low permeability reservoirs, Processes 12 (2024) 1476.
[26] Y. Tan, Q. Li, L. Xu, A. Ghaffar, X. Zhou, P. Li, A critical review of carbon dioxide enhanced oil recovery in carbonate reservoirs, Fuel 328 (2022) 125256.
[27] F.M. Orr, Jr, J.J. Taber, Use of carbon dioxide in enhanced oil recovery, Science 224 (1984) 563–569.
[28] S.-H. Cho, S. Jung, K.-Y.A. Lin, E.E. Kwon, Strategic use of CO2 in the catalytic thermolysis of bio-heavy oil over Co/SiO2 for the enhanced production of syngas, Energy Convers. Manag 222 (2020) 113195.
[29] X. Li, D. Yang, X. Sun, Y. Zhang, Characterization of phase structures of a supercritical water/supercritical carbon dioxide/heavy oil system with molecular dynamics simulations, Geoenergy Sci. Eng. 228 (2023) 211957.
30] S. Yang, H. Wang, X. Lou, Y. Pan, Z. Hu, Y. Yan, Asphaltene deposition inhibitors in CO2 flooding: a review and future application prospects, Energy Fuels (2024).
[31] M. Gao, G. Zhang, L. Zhao, J. Gao, C. Xu, Research progress of basic catalyst used in catalytic cracking for olefin production and heavy oil utilization, Ind. Eng. Chem. Res. 62 (2023) 1215–1226.
[32] B. Li, G. Liu, X. Xing, L. Chen, X. Lu, H. Teng, J. Wang, Molecular dynamics simulation of CO2 dissolution in heavy oil resin-asphaltene, J. CO2 Util. 33 (2019) 303–310.
[33] J.A. Miller, C.T. Bowman, Mechanism and modeling of nitrogen chemistry in combustion, Prog. Energy Combust. Sci. 15 (1989) 287–338.
[34] Y. Jean, F. Volatron, Theoretical models for activation of CO2 towards hydration (CO2+ H2O→ H2CO3) by cationic binding sites, Chem. Phys. 65 (1982) 107–111.
[35] S. Tanaka, H.H.J. Meiselman, E. Engel, P.H. Guth, O. Furukawa, R.B. Wenby, J. Lee, J.D. Kaunitz, Regional differences of H+ , HCO3−, and CO2 diffusion through native porcine gastroduodenal mucus, Dig. Dis. Sci. 47 (2002) 967–973.
[36] V. Simanzhenkov, R. Idem, Crude Oil Chemistry, CRC Press, 2003.
[37] A. GUO, Z. REN, L. TIAN, Z. WANG, K. LI, Characterization of molecular change of heavy oil under mild thermal processing using FT-IR spectroscopy, J. Fuel Chem. Technol. 35 (2007) 168–175.
[38] Y.I.I. Abdelsalam, F.A. Aliev, O.O. Mirzayev, S.A. Sitnov, V.E. Katnov, L. A. Akhmetzyanova, R.E. Mukhamatdinova, A.V. Vakhin, Aquathermolysis of heavy crude oil: comparison study of the performance of Ni (CH3COO) 2 and Zn (CH3COO) 2 water-soluble catalysts, Catalysts 13 (2023) 873.
[39] I.A. Wiehe, Process Chemistry of Petroleum Macromolecules, CRC Press, 2008.
[40] N.M.R. Basic, Nuclear Magnetic Resonance Spectroscopy, (2001).
[41] M. Balci, Basic 1H-and 13C NMR Spectroscopy, Elsevier, 2005.
[42] J.C. Poveda, D.R. Molina, Average molecular parameters of heavy crude oils and their fractions using NMR spectroscopy, J. Pet. Sci. Eng. 84 (2012) 1–7.
[43] L.F. Montes, E.C.S. Oliveira, Á.C. Neto, S.M.C. Menezes, E.R.V. Castro, L. L. Barbosa, Low-field NMR: a new alternative to determine the aromatic content of petroleum distillates, Fuel 239 (2019) 413–420.